Anode geometry influence on LaB 6 cathode discharge characteristics

G.-C. Potrivitu, S. Mazouffre, L. Grimaud, R. Joussot

▶ **To cite this version:**

G.-C. Potrivitu, S. Mazouffre, L. Grimaud, R. Joussot. Anode geometry influence on LaB 6 cathode discharge characteristics. Physics of Plasmas, 2019, 26 (11), pp.113506. 10.1063/1.5115834 . hal-02409739

HAL Id: hal-02409739
https://hal.science/hal-02409739v1

Submitted on 9 Feb 2022

HAL is a multi-disciplinary open access archive for the deposit and dissemination of scientific research documents, whether they are published or not. The documents may come from teaching and research institutions in France or abroad, or from public or private research centers.

L'archive ouverte pluridisciplinaire **HAL**, est destinée au dépôt et à la diffusion de documents scientifiques de niveau recherche, publiés ou non, émanant des établissements d'enseignement et de recherche français ou étrangers, des laboratoires publics ou privés.

Anode geometry influence on LaB_6 cathode discharge characteristics

G-C. Potrivitu,[a] S. Mazouffre,[b] L. Grimaud, and R. Joussot
[1] *CNRS, ICARE, UPR 3021, 1C av. de la Recherche Scientifique, CS 50060, F-45071, Orléans cedex 2, France*

(Dated: 11 September 2019)

The characterization of electric propulsion device cathode is performed in so-called diode configuration with an external anode. The anode acts as a physical boundary for the cathode plasma discharge, therefore it influences cathode operation and performances. In this study, four different anodes – namely a disk, a plate, a long and a short cylinder – have been used with a flat disk LaB_6 emitter 5 A-class cathode to examine the anode geometry impact on cathode discharge properties. Current-voltage curves, discharge oscillations, electron parameters and ion velocities have been measured for currents in the 2 A to 12 A range and xenon mass flow rates varied from 0.4 mg/s to 1 mg/s with a fixed cathode-to-anode distance. The set of results clearly supports the fact that the anode geometry strongly influences the cathode characteristics both at the macroscopic and the microscopic scale.

I. INTRODUCTION

Electron sources are key components for electrostatic thrusters such as gridded ion engines, FEEP thrusters and Hall thrusters[1]. For the first two devices, electrons solely serve for ion beam neutralization, therefore avoiding spacecraft charging and allowing for high performances and low beam divergence angle. In the case of Hall thrusters, a large fraction of electrons provided by the external source neutralizes the ion beam and the remaining part compensates for losses in the magnetized plasma discharges, therefore allowing for high efficiency and stable operation.

In the electric propulsion field, electron sources are termed neutralizers or cathodes. The source rests upon thermionic emission of electrons by a hot element often called the insert or emitter. Various materials can be used for insert, from refractory metals, such as tungsten, tantalum or molybdenum, to more complex ceramic materials, such as lanthanum hexaboride (LaB_6), cerium hexaboride (CeB_6) and porous tungsten impregnated with barium oxide (BaO-W) or calcium aluminate electride (C12A7:e^-) to only name a few[2,3].

As the cathode is a critical element for many electric propulsion devices, it requires optimization in terms of power and propellant consumption, as well as accurate characterization in terms of current–voltage curves, oscillation level and discharge mode before being coupled to a thruster[2]. For the investigation of a cathode in standalone configuration, *i.e.* without thruster, an external anode is needed to close the electrical circuit. The anode must in fact be seen as a physical boundary condition for the cathode plasma discharge. As a direct consequence, the anode position, surface and shape are parameters that govern to a certain extent the cathode discharge properties and behavior due to their impact on the current density balance and electric field topology. We recently carried out works on the influence of the cathode–anode distance upon cathode characteristics[4]. In this contribution, we highlight the issue of anode geometry influence on cathode discharge characteristics, as the latter is poorly documented in the open literature[5–7].

For this purpose a xenon-fed 5 A-class LaB_6 cathode has been tested in the so-called diode configuration with four different anode types in the 2 A – 12 A discharge current range. In spite of a relatively large work function around 2.6 eV, see Ref. 2 and references herein, LaB_6 stays a rational choice as emitter due to its low evaporation rate and robustness to impurity poisoning and water vapors. We first examined the macroscopic properties of the cathode plasma for xenon mass flow rates between 0.4 mg/s and 1 mg/s. The current-voltage curves of the cathode have been recorded using electrical probes. The plasma discharge mode, *i.e.* spot mode versus plume mode, has been visually inspected and identified according to the discharge current oscillation level[8,9]. Secondly, microscopic plasma properties have been investigated downstream of the cathode orifice. Singly-charged xenon ion velocity has been measured by means of near-infrared Laser-Induced Fluorescence (LIF) spectroscopy along the cathode axis. Electron temperature and density as well as plasma potential have been determined using a single Langmuir probe for several axial positions. Even though various anode geometries have been investigated in previous works, studies were independent with one anode type each time but in a few works[5–7], which makes comparisons and general conclusions difficult. The originality of this study lies is that here four different anode geometries are investigated with a single cathode and a fixed cathode-to-anode gap using the same vacuum chamber, identical power supply and gas feeding system and the same set of diagnostics tools. Moreover, the combination of LIF spectroscopy and Langmuir probe measurements is quite unique for cathode study.

All experimental results and related interpretations are presented and discussed in this article after a detailed description of experimental setup and measurement procedures.

[a] Currently at Nanyang Technological University, Singapore
[b] Corresponding author: stephane.mazouffre@cnrs-orleans.fr

II. EXPERIMENTAL ARRANGEMENT

A. Vacuum chamber

Experiments have been carried out in NExET (New Experiments on Electric Thrusters) vacuum chamber. The NExET chamber is a 0.8 m in diameter and 1.8 m in length stainless steel cylinder with grounded walls fit with dry, cryogenic and turbomolecular pumps. A pumping speed of about 8000 l/s can be achieved with a typical surface temperature around 35 K. During measurements the background pressure varied between 1 and 4×10^{-5} mbar depending on the xenon mass flow rate and the input power. In order to absorb a large fraction of the ion beam energy, water-cooled graphite tiles are placed at the back of the chamber, thus limiting the thermal load on the cryogenic surface. The chamber can be easily accessed via a 0.8 m in diameter door located at the front of the chamber. The vacuum chamber is equipped with several power, gas and plasma diagnostic feedthroughs as well as observation windows that provide view access to the interior.

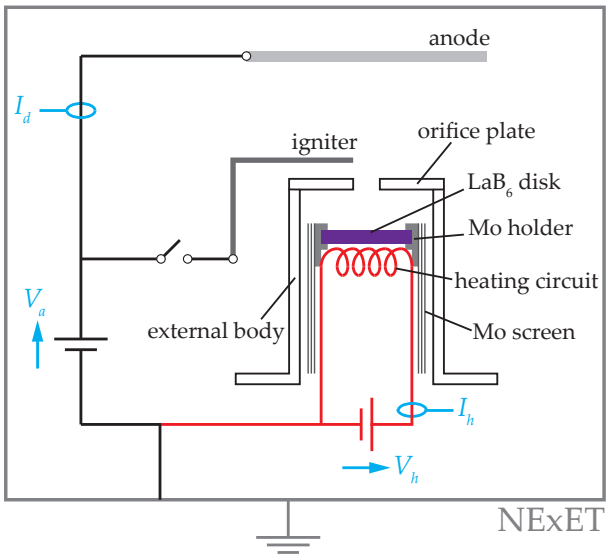

FIG. 1. Schematic of the cathode and simplified diagram showing electrical connections as well as main currents and voltages.

B. Cathode and anodes

The cathode used in this work is a laboratory model 5 A-class cathode with a flat disk shape LaB_6 insert heated by a tungsten filament. Although flat emitters are less common than cylindrical ones, such a geometry has been used by various groups in the past, mostly for fundamental works[4,10–14]. Only a brief description of the cathode is given here. More details about the cathode architecture and operation can be found in reference[11].

The LaB_6 insert is 8 mm in diameter and 2 mm thick. It is held in place by a molybdenum holder with a 6 mm in diameter aperture. Heating is ensured by a coiled tungsten filament located underneath the insert. Radiative losses are minimized thanks to a molybdenum screen which surrounds the filament-holder-insert assembly. As the required cathode lifetime is typically below 200 hours for such studies, no diffusion barrier was added between the insert and the Mo parts[15]. The cathode external body is a stainless steel cylinder with a 25 mm-diameter a 95 mm-length. The cathode orifice is 3 mm in diameter with a 1/3 aspect ratio, *i.e.* length to diameter ratio. A 0.1 mm thick pyrolytic graphite foil is placed between the orifice plate and the external body to warrant good sealing.

Xenon is supplied through a gas feeding line mounted to the external body. Cathode discharge ignition is here achieved using a positively biased external igniter placed 4 mm in front of the orifice. The cathode could be operated in self-sustained mode, that means neither external heating nor keeper current is applied after ignition, throughout the entire discharge current range spanned in this work. A schematic of the cathode along with electrical connections is shown in Fig. 1.

The cathode was tested in diode configuration with four different external anodes made of non-magnetic stainless steel. Two geometries have been selected: planar and cylindrical. They are the most common geometries for cathode discharge characterization in the electric propulsion field[16–18]. Two anodes have a planar geometry: one is a plate while the other one is a disk. The surface area ratio between the two anodes is about 4.3. Two anodes have a cylindrical geometry: one is a long cylinder while the other is a short cylinder. The two cylinders have the same diameter but a different length. Their surface areas correspond to the ones of the planar anodes. The main characteristics of the anodes as well as the cathode discharge conditions are summarized in Table I. Figure 2 illustrates the four anode geometry. During experiments, the anode was always located 20 mm away from the cathode exit plane (orifice). Besides, cathode and anode axis were aligned but for the plate. In the latter case the cathode axis was aligned with the hole center, see Fig. 2. Notice the flat anode was previously used for characterization of our cathode[11] and the disk anode was used in a study about the cathode to anode gap impact[4].

During envelope examination the chamber background pressure varied between 1.8 and 6.2×10^{-5} mbar, as displayed in Table II. During the Langmuir probe measurements, the background pressure was 3×10^{-5} mbar at a Xe mass flow rate of 0.6 mg/s, while during the LIF measurements the pressure varied between 2 and 4.4×10^{-5} mbar.

TABLE I. Anode geometry and cathode discharge conditions.

Geometry type	Anode	Surface area (cm^2)	Discharge current (A)	Mass flow rate (mg/s)
Planar	Plate	411.3		
	Disk	95	2 – 12	0.4 – 1
Cylindrical	Long cylinder	411.3	step of 2	step of 0.2
	Short cylinder	95		

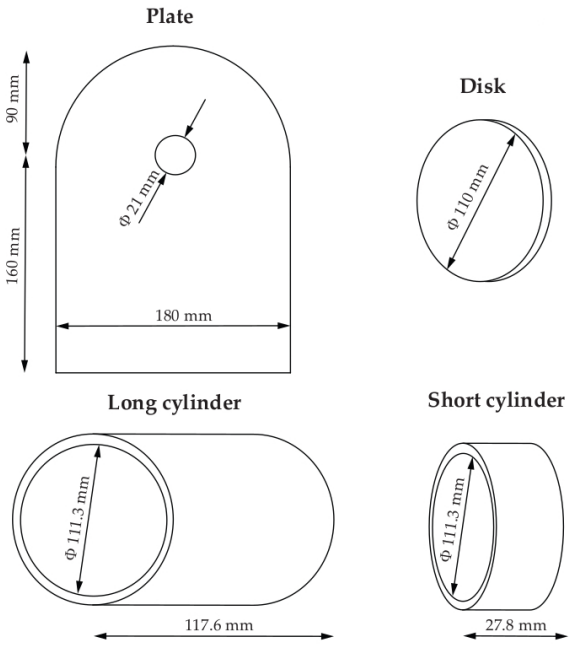

FIG. 2. Schematics of the four anodes used in diode configuration with the cathode.

TABLE II. Vacuum chamber background pressure. The Xe mass flow rate varies from 0.4 to 1 mg/s.

Anode	Pressure ($\times 10^{-5}$ mbar)
Plate	1.8 – 6.1
Disk	2.8 – 5.7
Long cylinder	1.8 – 5.4
Short cylinder	2.3 – 6.2

C. Electrical measurements

A layout of electrical connections is depicted in Fig. 1. The circuit of the cathode heater was connected to a 40 V–25 A power supply during the cathode heating sequence. The cathode–anode discharge was maintained by a 200 V-70 A (5 kW) power supply. The external igniter was connected to the same supply through a switch. The cathode external body was kept floating during all experiments. Several electrical probes were used in order to measure the cathode discharge electrical parameters. The anode voltage was measured using a Tektronix P6139A voltage probe while the discharge (anode) current was monitored using a Tektronix TCP202 current probe. The two instruments were connected to a Tektronix TDS5104 digital oscilloscope (1 GHz, 5 GS/s). Waveforms have been sampled at 1 MHz. This frequency is high enough to allow visualization of the main oscillating phenomena that the discharge current and voltage may exhibit during cathode operation, see Ref. 11 and references herein.

D. Working procedure

Before igniting the cathode–anode discharge, the LaB_6 emitter has to be heated to facilitate electron emission. The procedure is the following. The filament heating current I_h is slowly ramped up to 16 A. At that point the heating circuit potential V_h typically reaches about 14.5 V. The heating power delivered to the LaB_6 insert is therefore of about 230 W. After ignition of the discharge, the heating power is switched-off and the cathode operates in self-heating mode during measurements.

All experiments are conducted with the main discharge power supply working in a current regulated configuration. For each value of the discharge current I_d, the xenon mass flow rate is increased from 0.4 mg/s to 1 mg/s with a 0.2 mg/s step size, while the anode potential V_a is recorded. Here V_a is the potential difference between the anode and the insert. After each change in Xe mass flow rate or in discharge current, the cathode is operated during 600 s before any traces are recorded in order to warrant steady state operation of the cathode discharge.

E. Uncertainty analysis

Experimental data includes both systematic and random uncertainties. The measurement uncertainties are here estimated according to Abernethy *et al.*[19] and the error propagation law proposed by Kline and McClintock[20] is used. The systematic uncertainties include accuracy, stability, sensitivity, resolution, measurement error and linearization. The random uncertainty corresponds to the standard deviation of the experimental measurements. The general expression of the total uncertainty ΔR of an experimental quantity R, which is a function of several variables $\left(\overline{X}_1, \overline{X}_2, ..., \overline{X}_J\right)$, calculated in considering a confidence interval of 95% is defined as

follows[21]

$$\Delta R = \left[\sum_{i=1}^{J} \sum_{k=1}^{K} \left(\frac{\partial f}{\partial X_i} \Delta \overline{X}_i^k \right)^2 + \sum_{i=1}^{J} \left(t_{95} \frac{\partial f}{\partial X_i} X_{i,std} \right)^2 \right]^{1/2}, \quad (1)$$

where $\Delta \overline{X}_i^k$ is the k-th type of systematic uncertainty of the i-th variable, t_{95} is the quantile of a two-tailed Student's t-distribution with a confidence interval of 95%, and $X_{i,std}$ is the standard deviation (unbiased estimator) of the i-th variable. When measurement of R is repeated N times, t_{95} is divided by $N^{1/2}$ and the standard deviation of the N measurements is considered instead of $X_{i,std}$[21]. In this work, error bars shown in I-V plots represent the total uncertainty calculated with Eq. (1).

The total uncertainty of the discharge current/anode potential, see section III, takes into account sources of measurement uncertainty found in manufacturer data sheets: power supply accuracy (0.2% / 0.1%) and regulation (0.2% / 0.07%), probe accuracy (3% / 0.5%) and sensitivity (40 mA / na), oscilloscope resolution (8 bits) and accuracy (1.5%).

The total uncertainty in position for LIF and Langmuir probe measurements, see section IV, takes into account accuracy (18 μm), repeatability (5 μm) and backlash (30 μm) of the translation stage, estimated uncertainty due to positioning of Langmuir probe and LIF collection optics (0.1 mm) as well as spatial resolution of the Langmuir probe (2 mm) and the LIF setup (200 μm). Errors in LIF and Langmuir probe signals are discussed in section IV.

III. CATHODE DISCHARGE CHARACTERISTICS

A. Operating envelopes

The evolution of the anode potential as a function of discharge current is presented in Fig. 3 for the four anode geometries and for various xenon mass flow rates. When no data point is shown, either the plasma discharge was too unstable or the applied power limitation was reached. As a general tendency, the anode potential decreases when the gas mass flow rate is increased whatever the geometry, as expected[22]. The short cylindrical anode gives the highest potential, especially at low mass flow rates. The three other anodes, *i.e.* plate, disk and long cylinder, exhibit roughly the same discharge characteristics and trends. In brief, a reduction in the anode potential is observed as the discharge current is increased, as described in other works[23], which exemplifies a decrease in the plasma electrical resistance. Moreover, the difference in anode potential between the various designs increases with the increase in mass flow rate for a discharge current above 6 A. The negative discharge impedance, *i.e.* reduction in anode potential with increase in discharge current, can be explained by a decrease in the emitter sheath potential, as explained in Ref.[24]. The consequence is a higher ion energy flux delivered to the emitter wall, which permits the increase in thermionic emission needed for the higher discharge current imposed.

For the majority of tested points, the measured difference in anode potential is higher than the standard deviation, which indicates that the anode geometry influences the discharge characteristics. The short cylindrical anode has in particular the largest potential whatever the mass flow rate. The lowest potential is obtained with the plate-shape anode for most cases above 6 A. For the three other geometries, the situation depends on the discharge current but the gap in potential is moderate. As can be seen in Fig. 3, two domains can be distinguished, below and above 8 A. Interestingly, the overall results show that the shape of the anode has a strongest impact than the surface area.

The discharge electrical resistance, *i.e.* ratio of the anode voltage to the discharge current, decreases with the discharge current up to 8 A for all cases. This fall is followed by a relatively constant discharge electrical resistance, as the current is further increased. The short cylindrical anode displays the highest discharge electrical resistances for the entire range of discharge current.

An example of cathode discharge current power spectrum is shown in Fig. 4 for the plate anode. When analyzing power spectra, one finds that plasma discharges, when the cathode operates in plume mode, are characterized by frequencies of the fundamental peak in the range 20 to 80 kHz whatever the geometry. This is in agreement with previous results[4,11]. Moreover, the fundamental frequency seems to increase with the discharge current, the spectra becoming more energetic, and to decrease when the mass flow rate is increased. This behavior was previously reported in the literature[18,25,26]. This range of discharge current frequencies in power spectra suggests the existence of ionization-like instabilities in the cathode plume[26–29].

B. Discharge modes

Cathode discharge modes and mode transition are described by several theories[8,9,30]. One of them suggests that when the passive current to the anode, *i.e.* the steady state thermal electron current, is not sufficient to sustain the desired discharge current, electron attracting sheaths form at the anode location and increase the collected current[30]. This usually happens at low mass flow rates or low discharge current. The low plasma density in the cathode plume at low mass flow rates or low discharge current cannot generate the necessary thermal electron current and a constricted attachment of the cathode plasma plume to the anode is observed[9,31,32]. Visually, the cathode plasma plume in spot mode presents

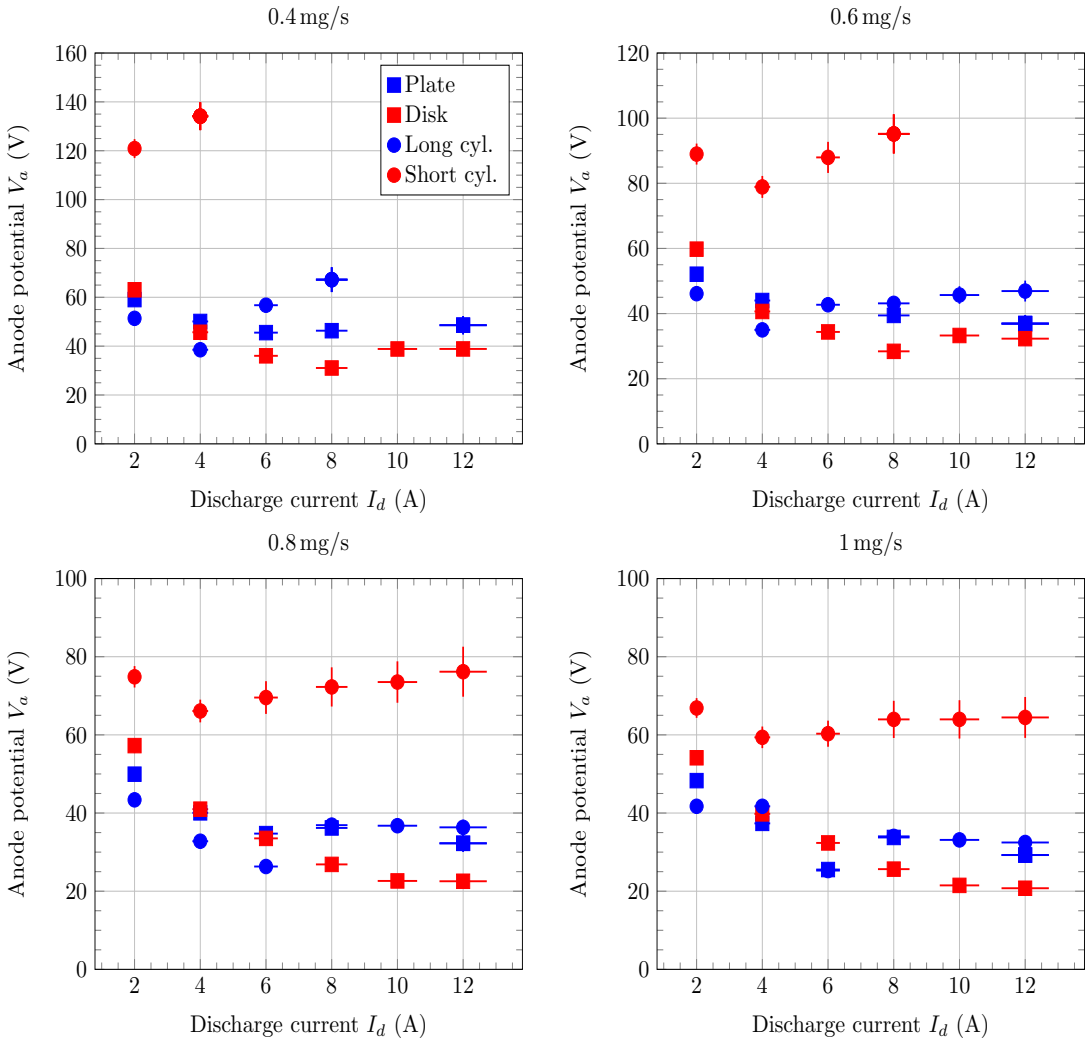

FIG. 3. Anode potential V_a against discharge current I_d for the various anode geometries when the xenon mass flow rate is varied from 0.4 mg/s up to 1 mg/s.

a bright, spot-like structure ahead of the cathode orifice with a blue coloring due to the high density of xenon ions[4]. Fast electrons produced by the cathode in this operating regime induce ionization and excitation of neutral atoms near the cathode exit plane, while the rest of the cathode–anode space remains dark[30]. In contrast, when in plume mode, the cathode displays a bright high divergence plasma plume that extends far downstream[4]. The plume is purple, a color that characterizes the presence of a large amount of excited xenon atoms instead of ions. Ionization and excitation events occur predominantly in the far field plume owing to fast electrons escaping the sheath formed in front of the orifice[30]. High temporal fluctuations of the anode potential are observed in plume mode[11].

A common criterion to distinguish between the spot and plume mode operation relies on the discharge current oscillation level. Spot mode operation is associated with a ratio between the discharge current standard deviation $I_{d,std}$ and the discharge current mean value I_d below 9 %. Ratios above this threshold indicate plume mode discharges[33]. Figure 5 depicts the cathode discharge modes observed with the four anodes according to the aforementioned criterion.

As can be seen in Fig. 5*a*, planar anodes operates in spot mode for discharge currents below 6 A with weak fluctuation level of electrical parameters, typically below 2% of the mean value. However, in spot mode the anode potential in large. The plume mode is observed for high discharge currents. The spot to plume transition occurs at $I_d = 6$ A. At this current, the cathode is in plume mode for mass flow rates ≤ 0.6 mg/s and in spot mode for mass flow rates > 0.6 mg/s.

For low mass flow rates (0.4 and 0.6 sccm), the disk-shape anode runs in spot mode for discharge currents < 8 A and in plume mode above 8 A. For larger mass flow rates the cathode runs in spot mode over the entire range of discharge current. Discharge current oscillations

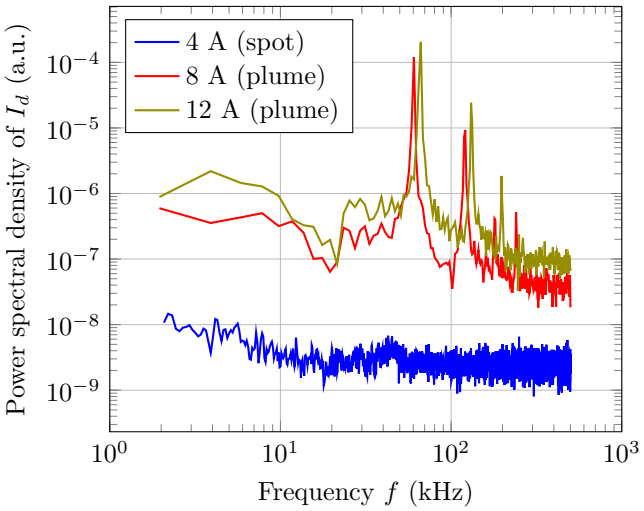

FIG. 4. Power spectrum acquired with the plate anode when the cathode operates at 4, 8 and 12 A with 0.6 mg/s of xenon.

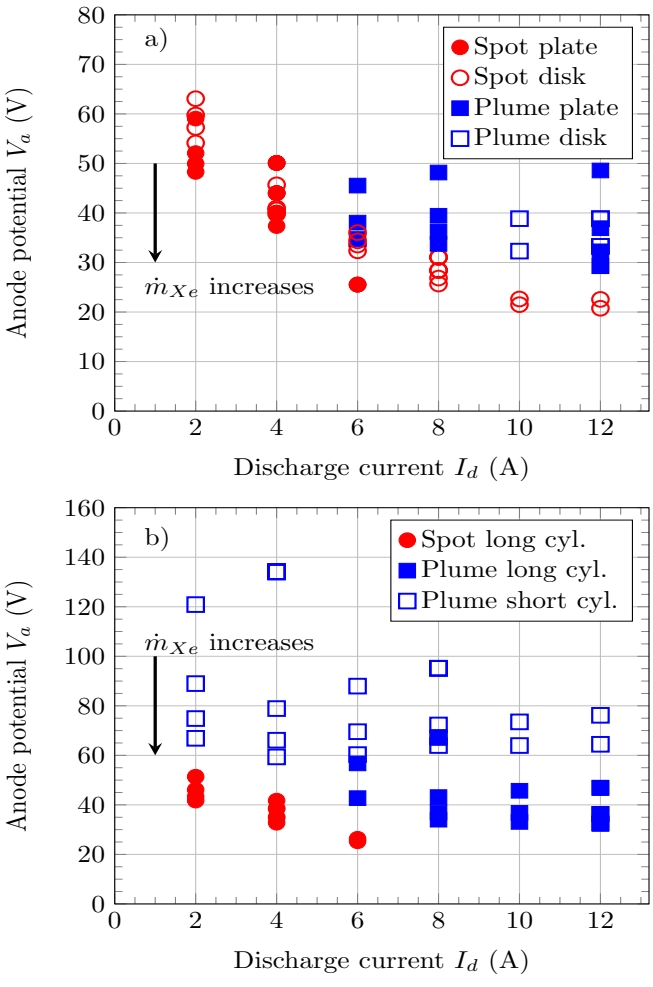

FIG. 5. Cathode discharge mode map for *a)* planar anodes and *b)* cylindrical anodes. The xenon mass flow rate ranges between 0.4 mg/s and 1 mg/s.

are below 2 % and of about 10 % in spot and plume mode, respectively.

Fig. 5*b* depicts the results for cylindrical anodes. The long cylindrical anode behavior is quite similar to the plate. For I_d below 6 A, the cathode is in spot mode with fluctuations lower than 5 %. However, in spot mode the anode potential for the long cylinder is lower than the one of the plate. As the discharge current is ramped up, the cathode transitions to plume mode with $I_{d,std}/I_d$ ratios between 10 % and 40 %. In like manner, at $I_d = 6$ A the cathode is in plume mode at low mass flow rates and in spot mode at large mass flow rates.

The short cylindrical anode operates only in plume mode, see Fig. 5*b*, with an average anode potential of 80 V. Fluctuations of electrical parameters range between 20 % and 36 %. They increase with the discharge current and decrease with the mass flow rate.

To summarize, depending on both the anode geometry and the operating parameters, the cathode can operate either in spot mode or in plume mode:

(i) *spot mode at low discharge current*: Usually the anode potential is high and it diminishes with the increase in mass flow rate or the increase in discharge current.

(ii) *plume mode at high discharge current*: Usually the anode potential is low; the only exception is the short cylindrical anode where high anode potentials are recorded in plume mode at high discharge current. This mode has been previously observed at low mass flow rates and denoted as "diffuse mode"[25].

(iii) *spot mode at high discharge current*: Classic case according to the literature[30]. The anode potential is low. It is the case of the disk at high mass flow rates;

(iv) *plume mode at low discharge current*: Classic case according to the literature[30]. The anode potential is high.

It is worth adding that visual inspection reveals a plasma plume shape and luminosity quite different from the standard description[2,8,30]. In spot mode, instead of a single, bright, spot-like structure in front of the cathode orifice, the external plasma discharge is spread out and diffusely attached to the anode. In plume mode, the plasma plume is strongly divergent and distinctively composed of a bright region at the cathode exit plane and a less bright, more diffuse region attached to the anode. The two regions are separated by a dark space[11,18,25,34,35]. The dark space size and position with respect to the cathode orifice change when the mass flow rate increases or the discharge current varies. Those particular features of the cathode discharge plume have been previously presented and discussed[4].

IV. ION AND ELECTRON PROPERTIES

A. Diagnostics

The singly-charged Xe^+ ion Velocity Distribution Function (VDF) has been measured along the cathode axis downstream the orifice by means of Laser-Induced Fluorescence (LIF) spectroscopy for several cathode–anode configurations. The enclined reader can find information about LIF principle, associated optical train and data analysis in Refs. 36 and 37. Only a brief description of the setup is given here.

The $5d^4F_{7/2} \rightarrow 6p^2D^0_{5/2}$ transition of metastable Xe^+ ions at 834.7 nm is excited by a continuous infrared narrowband laser beam. A 50 μm diameter optical fiber carries the ligth into the vacuum chamber. A Fabry-Pérot interferometer and a high finesse wavemeter are used to verify the mode quality and measure the wavelength, respectively. The uncertainty in velocity is here around ± 60 m/s[38]. The fluorescence radiation is collected by a lens that focuses light into a 200 μm diameter optical fiber. The light is then transferred to a monochromator tuned to the 541.9 nm fluorescence wavelength. A photomultiplier tube and a lock-in amplifier set at the beam modulation frequency provide the final signal.

The entire cathode-anode assembly was installed on a remotely controlled linear translation stage to permit spatially resolved measurements. To avoid formation of "ghost" VDF due to laser beam reflection[38], the cathode was tilted upwards at a 13° angle with respect to the anode axis.

A cylindrical single Langmuir probe was used to determine the electron properties in the cathode plume on the axis[4,39,40]. The probe collection part is a 0.15 mm in diameter and 2 mm in length tungsten wire. The rest of the wire was insulated from the plasma by a 100 mm long and 1.5 mm in diameter alumina tube. The voltage sweep and the resulting probe current measurement were performed using an automatic system (Impedans ALP System). The probe was mounted onto an $x-y$ translation stage to locate the tip at the desired location in the cathode plume, as depicted in Fig. 6. For all measurements the probe tip was parallel to the plasma flow.

B. LIF spectroscopy results

Due to the presence of several abundant xenon isotope, recorded fluorescence lineshapes do not correspond to the real ion VDF[36,37]. However, the Doppler shift of the lineshape indicates the ion velocity and the width provides information on the ion temperature in the direction of interrogation. As the laser beam does not propagate exactly on the cathode axis, the measured magnitude of the ion axial velocity is slightly underestimated in this work. The area of the lineshape gives the relative density of

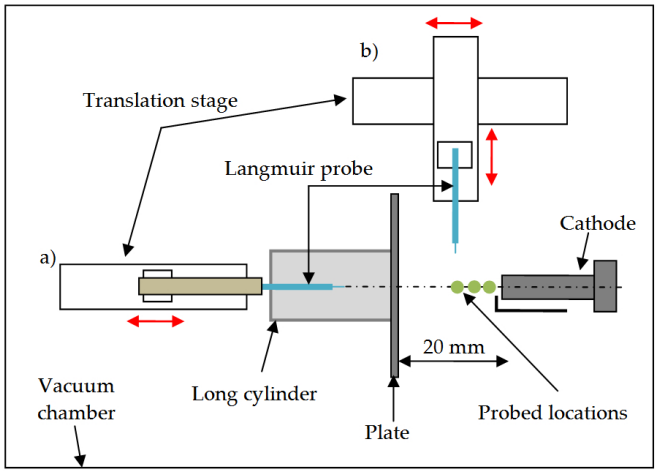

FIG. 6. Schematic of the Langmuir probe setup in the case of *a)* the long cylinder and *b)* the plate.

xenon ions in the probed metastable state. Note that raw lineshapes have been smoothed using a fourth order Butterworth filter and a moving average Savitzky-Golay filter prior to analysis.

The Xe^+ ion VDF has been studied with the plate-shape and the long cylindrical anodes. The two configurations were set in spot mode at 4 A and 0.6 mg/s. Additional LIF results were obtained with the plate in plume mode at 10 A and 0.6 mg/s.

Figure 7*a* shows the evolution of the normalized ion VDF as a function of the axial position using the plate as anode with a discharge in spot mode. The anode potential was 46 V and current fluctuations were around 1.4 %. Contrary to what was observed in the past with a similar hollow cathode[41], several ion groups can clearly be distinguished in Fig. 7*a*. The group with the largest population has a positive mean velocity that means ions move towards the anode. The velocity does not change much with the distance to the cathode orifice. The temperature of the dominant group slightly decreases when moving downstream of the cathode exit plane. Below $x = 4$ mm a non-negligible fraction of the ion population flows towards the cathode as a significant peak with a negative velocity can be seen in Fig. 7*a*.

Figure 7*b* shows the ion VDF for several positions in the case of the long cylindrical anode with a discharge in spot mode. The anode potential was 50 V and the current oscillation level reached about 2.5 %. The VDF is here composed of either a single peak or two peaks like at $x = 1, 3, 4$ and 5 mm. Whatever the shape of the distribution, one can distinguish ions with positive velocities and ions with negative velocities. The mean velocity of the group of ions that flow towards the cathode does not vary much with the position, as with the plate anode. Its magnitude is -0.8 km/s for the plate and it is around -1.5 km/s for the long cylinder. Contrary to the plate anode case, the mean positive velocity increases fast when the distance to the cathode orifice increases and its

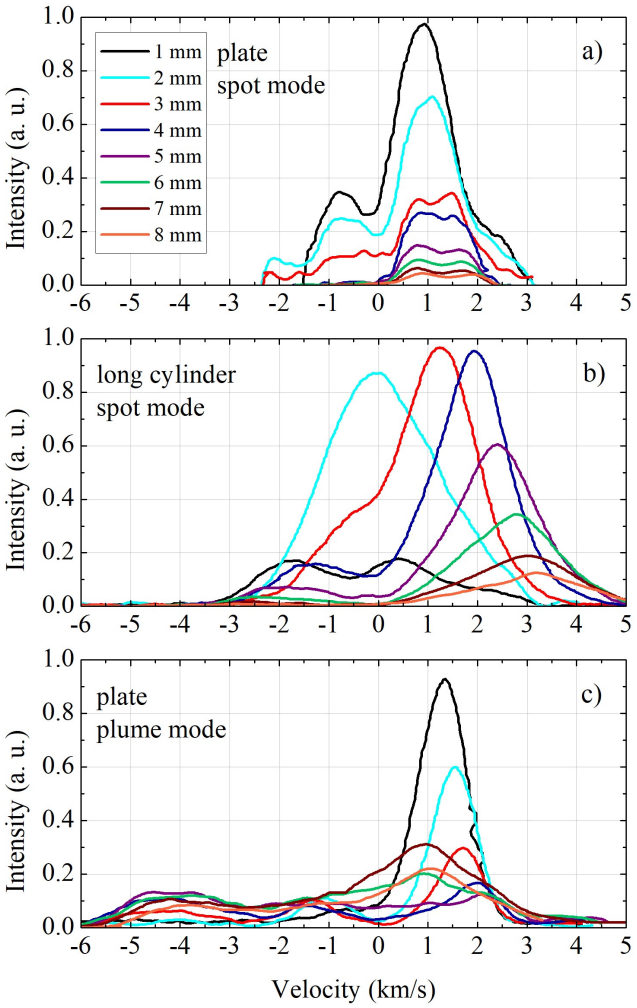

FIG. 7. Ion VDF for various positions in the cathode-to-anode gap ($x = 0$ refers to the cathode orifice) for *a)* the plate in spot mode, *b)* the long cylinder in spot mode and *c)* the plate in plume mode. The cathode-to-anode distance is 20 mm.

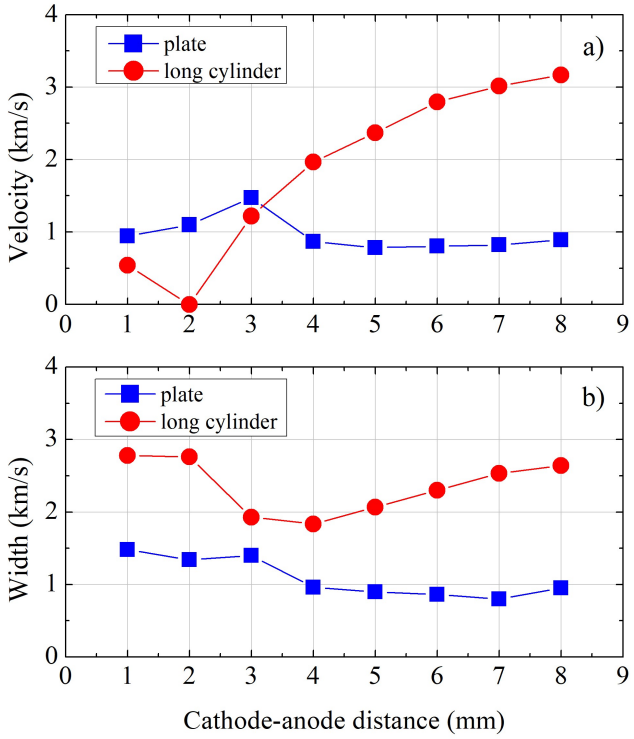

FIG. 8. Most probable velocity *a)* and distribution width *b)* of the main ion group against the cathode-to-anode distance for two anode geometries. The discharge works in spot mode for both anodes.

value is larger, 3 km/s against 1 km/s. The most striking difference between the two configurations is the velocity spread, as can be seen in Fig. 7*a* and 7*b*. The width of the VDF is much larger with the cylindrical anode. Moreover, after a drop over the first 4 mm, the width increases until $x = 8$ mm, which suggests an increase in the ion temperature as one nears the anode. A similar trend has already been found in experiments and simulations with a high-current hollow cathode coupled to a cylindrical anode[42–44]. The increase in temperature was then explained through the presence of ion acoustic turbulence (IAT). Since the discharge current is low in our study (under 12 A), it is unlikely that IAT would be the main mechanism for ion heating. The broadening of the ion VDFs might originate from the relatively high level of discharge current fluctuations with the cylindrical anode (2.5 %) compared to the planar anode (1.4 %). Temporal fluctuations of the VDF translate into a broad distribution when performing time-averaged LIF measurements, hence an apparent heating. The presence of ions with negative velocities, however, is real. It cannot be the consequence of temporal average. Negative velocities certainly reveal fluctuations of the local plasma potential. Noticed that for cylindrical anodes ions could have a large radial velocity component, especially in the vicinity of the anode as the collecting surface is further away from the discharge centerline compared to planar anode case. Here the LIF setup was used to solely interrogate the axial velocity component so no information is available in the radial direction.

The most probable velocity of the main ion group of the distribution, *i.e.* the peak with the largest population, is depicted in Fig. 8*a* for the plate and long cylinder with a discharge in spot mode. Firstly, the most probable velocity is positive whatever the location and configuration, in agreement with previous works on a 5 A-class hollow cathode[41]. Secondly, the velocity is almost constant for the plate anode whereas it increases towards the anode for the long cylinder. Thirdly, the velocity is larger with the cylindrical anode. At $x = 8$ mm, the velocity reaches $\sim$ 3 km/s and $\sim$ 1 km/s for the cylinder and the plate, respectively. Finally, the width of the main VDF is larger with the long cylinder as can be seen in Fig. 8*b*. The width corresponds here to the full-width at half maximum of the main peak. LIF measurements

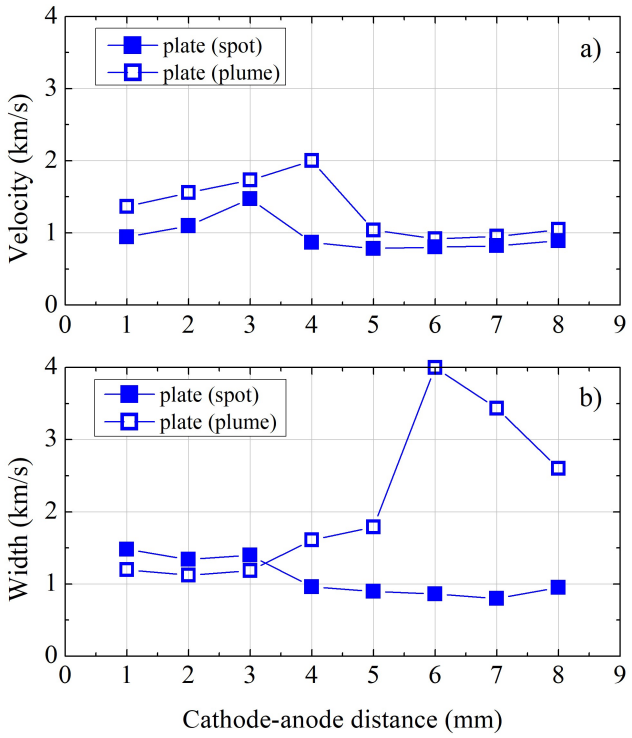

FIG. 9. Most probable velocity *a)* and distribution width *b)* of the main ion group against the cathode-to-anode distance for the plate anode with a discharge in spot mode (full square) and plume mode (open square).

carried out in the plume of a hollow cathode fired at 6 A (0.4 mg/s xenon) with a 63.5 mm cylindrical anode placed 2 mm downstream of the cathode exit plane revealed ion velocities up to 4.5 km/s[41]. Results are in the range of velocities found in this study for the long cylindrical anode.

In order to examine the impact of discharge fluctuations on the LIF lineshapes, the cathode was operated in plume mode with the plate anode at a discharge current of 10 A and a Xe mass flow rate of 0.6 mg/s. Discharge current fluctuations reach about 13 % of the mean value, while the anode potential is 39 V. The corresponding ion VDFs are presented in Fig. 7*c*. Ion velocities spread over a very broad range compared to the spot mode. In particular ions with high negative velocities, therefore moving towards the cathode, are present: velocities reach up to -5.5 km/s in plume mode against -2.5 km/s in spot mode. The mean velocity of the main ion group, however remains positive.

The change in velocity and dispersion with the distance from the cathode orifice are shown in Fig. 9*a* and 9*b* for the two modes. The most probable velocity of the dominant ion group is not impacted by the discharge regime. The velocity increases slightly in the first mm before decreasing to about 1 km/s. The width of the main peak is much larger in plume mode at locations greater than 4 mm downstream the cathode orifice, which indicates a larger ion temperature as noticed by Williams and co-workers[41]. Plume mode is known to exhibit higher plasma densities in the cathode-to-anode region and this is supported by the measured broader ion VDFs. Moreover, plume mode operation is characterized by the emergence of ionization-like instabilities and IAT, previously described and characterized by several teams[42,45]. In our case, the discharge current for the plume mode is relatively low for IAT to be present. Nevertheless, the existence of coherent, ionization-like instabilities is a mechanism that can explain, by its own, the increase in ion temperature for the plume mode case compared to the spot mode.

Ion production and acceleration mechanisms are likely identical whatever the anode geometries and discharge regimes. Slow ions can originate from ionization or charge-exchange collision events as suggested by Williams *et al.*[42]. The origin of fast ions with kinetic energies up to ~ 20 eV traveling in the two directions and hot ions with temperature around 2 eV remains unclear. The creation of a potential hill downstream of the cathode orifice has been proposed[41]. Some authors suggested the effect of a Lorentz force due to the self-induced magnetic field[46]. But it certainly has a negligible impact with our mass flow rate and current. IAT[42,45] is another possibility. Finally, the neutral gas pressure can also impact ion properties. A cylindrical anode geometry constricts less the neutral flow downstream of the cathode orifice, therefore the neutral density can be lower compared to a planar anode. A low neutral density impacts charge-exchange, ionization, excitation and recombination collision events in the cathode plume, which influences ion energy. Lower collision probabilities lead to larger temperature and velocity, what is obserbed for the cylindrical anode in Fig. 8.

C. Langmuir probe results

The current–voltage traces of the Langmuir probe have been recorded using an automatic system (Impedans ALP System). The plasma potential V_p corresponds to the maximum of the I–V curve first derivative. The electron current was obtained after subtracting the ion current from the total probe current. The electron energy distribution function (EEDF) was determined from the electron current trace second derivative taken between floating and plasma potential[39,47–50]. The electron density n_e is given by the zero order moment of the EEDF and the electron temperature T_e is inferred from the second order moment.

Assessment of the error bars for n_e and T_e is a rather complicated task[51]. Uncertainties depend on probe geometry, probe theory, acquisition system, measurement procedure and data treatment. In this work, the accuracy of the plasma potential is estimated to be around 10 % from a statistical analysis[52]. In the remainder of this section a relative uncertainty of $\pm 50\%$ and $\pm 30\%$

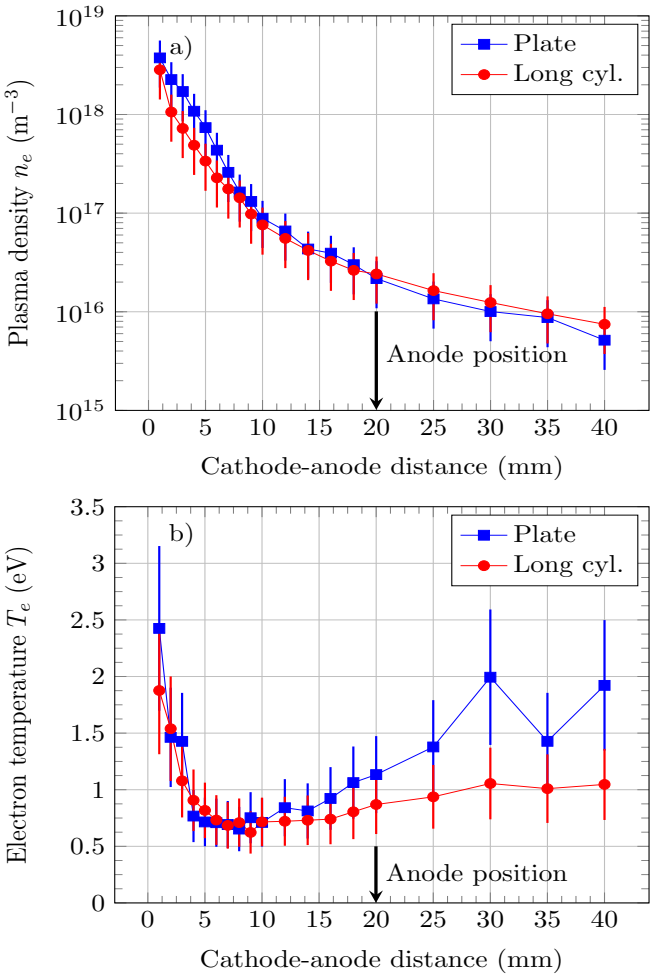

FIG. 10. Electron density *a)* and temperature *b)* against the cathode-to-anode distance for two anode geometries. The discharge is in spot mode.

is considered for the electron density and temperature, respectively[53].

Langmuir probe measurements have been carried out with the plate and the long cylindrical anode at 4 A with a Xe mass flow rate of 0.6 mg/s. The cathode discharge was in spot mode in the two cases. The development of the electron density along the cathode center-line is displayed in Fig. 10*a*. Electron number density varies from 4×10^{18} m^{-3} at the cathode exit plane down to 5×10^{15} m^{-3} at 40 mm downstream of the cathode orifice. Differences are noticed between the planar anode and the cylindrical anode especially in the first 10 mm. The density is higher for the plate anode. A geometry-induced constriction effect within the cathode-anode space could explain this result. Downstream of $x = 20$ mm, *i.e.* anode edge, the plasma density seems independent of the anode geometry.

The profile of the electron temperature T_e along the cathode axis is depicted in Fig. 10*b* for the two anodes. The trend is similar for the two anodes. A steep drop in electron temperature is observed over the first 5 mm of the plume, from around 3 eV to less than 1 eV. The decrease in both the electron density and temperature downstream of the cathode orifice is due to expansion of the plasma into a low pressure medium. In other words, the decrease is purely a geometrical effect[54]. Within the region between 5 mm and 15 mm T_e remains constant, with a value around 0.7 eV for the two anode geometries. Downstream of 15 mm from the cathode orifice, the temperature increases slowly even in the far downstream region. It reaches about 1 eV at the anode border, *i.e.* 20 mm, for the two configurations whereas the electron density still diminishes. For the long cylindrical anode, T_e increases very slowly downstream the anode edge. The increase is more pronounced for the plate anode as can be seen in Fig. 10*b*. The increase in temperature downstream of 20 mm from the cathode orifice might have too distinct origins. The first one is collisions with atoms of the background gas. The gas pressure can be relatively large in the downstream region as the anode acts as an obstacle for the gas flow. The second one is the existence of an electric field. In that case the field topology and magnitude would be different for the two anode geometries. However, as the plasma potential remains flat in the anode region, see next paragraph, the electric field, if any, is weak. Pressure effect is then the preferred explanation for the temperature increase.

Figure 11 shows the plasma potential V_p as a function of the cathode-to-anode distance. The plasma potential stays relatively constant in the covered domain but in the first 3 mm where a small decrease is observed as the consequence of plasma expansion. The plasma potential is lower for the long cylindrical anode, around 30 V. With the plate anode the potential reaches about 35 V on the average. The difference is in agreement with the anode potential, see Fig. 3. With the plate anode, the anode potential stabilized around 46 V, while with the long cylindrical anode the potential stabilized around 30.5 V. For the cylinder case, the plasma potential decreases by about 3 eV over the first 10 mm as shown in Fig. 11, which corresponds to a xenon ion velocity of 2.1 km/s assuming a collisionless medium. This number is in agreement with the measured ion acceleration. On the contrary, a rather constant plasma potential was measured for the plate anode and the increase in ion peak velocity is weak.

In a preceding study with a xenon-fed hollow cathode performed with two different anode geometries, a cylinder and a disk respectively, Qin and co-workers shown that the plasma potential was larger in the case of the cylindrical anode under identical operating conditions[5]. They also found a decreasing electron density within a small gap for the two anode geometries. Although plasma parameters obtained by Qin *et al.* differ from ours, their study clearly indicates that both the anode geometry and the cathode-to-anode distance influence the cathode functioning, in agreement with outcomes of this study and a previous one[4].

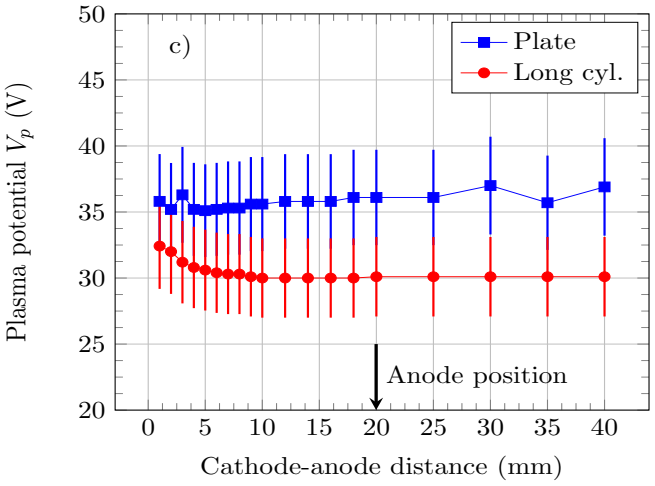

FIG. 11. Plasma potential as a function of the cathode-to-anode distance for two anode geometries.The discharge is in spot mode with an anode potential of 45 V for the plate and 30.5 V for the long cylinder, respectively.

V. DISCUSSION

In diode configuration, once the discharge is established, the current density at the cathode emitter j_e can be seen as the algebraic sum of several current densities[55], namely

$$j_e = \frac{I_d}{A_{emission}} = j_i + j_{em} - j_{th}, \tag{2}$$

where $A_{emission}$ is the emission surface area, j_i is the ion current density collected at the emitter surface, j_{em} is the electron thermionic current density and j_{th} is the electron thermal flux. Both ion current and electron thermal flux originate from the cathode and orifice plasma. The electron thermionic current density is a function of the sheath potential Φ_{sh}, due to the Schottky effect included into the Richardson-Dushman law. The sheath potential at the emitter surface changes with the local plasma properties, *i.e.* with the Debye length λ_D, and the plasma potential V_p[12]

$$\Phi_{sh} = \sqrt{\frac{eV_p}{\pi\epsilon_0\lambda_D}}. \tag{3}$$

At the anode surface two cases must be considered. When the anode potential V_a is lower than V_p an electron repelling sheath is formed and the cathode plume exhibits a diffuse attachment to the anode surface. The cathode then operates in spot mode[32]. Under those conditions, the current density balance at the anode j_a is[31]

$$j_a = \frac{I_d}{A_{collection}} = j_{th} - j_i - j_{em}, \tag{4}$$

where $A_{collection}$ is the current collection surface area at the anode. In spot mode, the collected electron current, *i.e.* the electron thermal flux, is a function of the potential barrier at the anode surface[32]

$$j_{th} = \frac{1}{4} n_e v_{th} \exp \frac{-(V_p - V_a)}{T_e}, \tag{5}$$

where v_{th} is the electron thermal velocity, n_e and T_e are the plasma density and electron temperature in the anode region, respectively. At saturation, when $V_a = V_p$, the thermal electron current density defined in Eq. (5) becomes

$$j_{th,sat} = \frac{1}{4} n_e v_{th}. \tag{6}$$

Therefore in spot mode the relation $j_{th} < j_{th,sat}$ is always satisfied. When the anode potential V_a is larger than V_p an electron attracting sheath is formed at the anode surface and the relation $j_{th} \geq j_{th,sat}$ is fulfilled. The cathode discharge plume exhibits a constricted attachment to the anode[32], and the cathode operates in plume mode in that case.

The cathode discharge can be seen as a complex system with several physical variables, such as emitter and anode currents, electrode surface areas and plasma property in the vicinity of the emitter and the external anode. The anode geometry influences the plasma properties in its vicinity, which in turn have an impact on the overall cathode discharge properties. Experimental results obtained in this study clearly show the anode geometry affects the cathode *I-V* envelope, the operating mode and the mode transition, the electron density and temperature, and finally the ion energy.

According to Eq. 4, for a certain value of the discharge current, I_d, and assuming a constant emission current density, j_{em}, a smaller collection area at the anode, $A_{collection}$ induces an increase in $(j_{th} - j_i)$, whereas a larger collection area may correspond to an increase in the same term. Therefore, the collected thermal electron current density, jth can be influenced by the anode surface area and as a consequence the spot/mode cathode discharge mode can be associated with the anode surface. In short anode geometries with small surface area are more prone to induce plume mode operation at similar discharge conditions. This can be seen when looking at the cylindrical anodes case: the long cylinder anode imposes plume mode operation for 54.5 % of operating points, while the short cylinder always leads to plume mode operation. However, the situation is the opposite for the planar anodes. The cathode operates in plume mode for 16.6 % of operating points with the disk anode (small area), while for the plate 55 % of points are in plume mode.

It was shown that plasma parameters differ for a cylindrical, hollow geometry and a planar one. LIF measurements revealed that a cylindrical geometry imposes higher ion velocities in the cathode plume, while the ion temperature tends to increase as approaching the anode, as shown in Fig. 8. Such characteristics of the cathode ion population suggest the emergence of coherent

ionization-like instabilities, specific to the plume mode operation. Moreover, a planar geometry with no holes, that constricts the neutral flow, as it is the case of the disk anode, can induce higher electron densities in the cathode-anode region and in turn maintain a thin plasma sheath at the anode, for a stable, spot mode operation. It is not surprising that the disk anode, although having a smaller surface area than the plate, imposes stable spot operation for more than 83 % of the operational points. The cathode-to-anode distance can also be discussed when planar or cylindrical geometries are considered as obviously this distance is larger for cylinders due to their 3D shape. It was previously showed that the cathode discharge mode transition is highly dependent on the cathode-anode distance, a higher distance inducing plume mode operation[4]. In a nutshell, for a sufficient large surface area, as it is the case of the plate and long cylinder, the anode geometry does not strongly influence the discharge mode, although plasma properties are affected. Besides, for a small surface area, as with the disk and short cylinder, a hollow geometry negatively impacts the cathode discharge by favoring mainly plume mode operation.

The external anode acts as a physical boundary for the cathode plasma discharge in diode configuration. In addition to being a physical boundary for the cathode plasma plume, the external anode also drives to a large extent the discharge current balance through its collection surface and its influence on the electric field topology. For instance, for a given emission current, there is a minimum anode surface area for maintaining the current balance, and hence a stable discharge. The shape of the anode also modifies the "view factor" from the cathode orifice, which influences the electron and ion fluxes, and hence the plasma properties in the cathode-anode gap.

VI. CONCLUSION

In this study, a flat disk LaB_6 emitter 5 A-class cathode was tested in diode configuration with four different external anodes in order to examine the anode geometry influence on the cathode discharge characteristics. The cathode was operated from 2 A to 12 A while the xenon mass flow rate was varied from 0.4 mg/s to 1 mg/s.

The anode geometry strongly influences the cathode operating envelopes and discharge mode distribution. For instance, the short cylindrical anode imposes the highest anode potential, while the cathode exhibits only plume mode operation for all discharge currents and mass flow rates. For the other three anodes, the spot mode is observed at low discharge currents and the plume mode is reached at high discharge currents. Moreover, differences have been noticed in ion and electron properties between plane and cylindrical geometries. Our set of results greatly supports the fact that the anode geometry influences cathode discharge characteristics both at the macroscopic and the microscopic level.

This work, along with our previous work on the cathode-anode gap impact on cathode characteristics, points out the need for standardization of cathode testing and performance measurements in the field of electric propulsion for spacecraft. This implies in particular the definition of common rules for cathode-anode gap and external anode geometry selection. Besides, it appears that the anode geometry should be included into cathode models and numerical simulations to better match the real experimental arrangement.

ACKNOWLEDGMENTS

This work was financially supported by the Région Centre and the French space agency (CNES).

[1]S. Mazouffre, "Electric propulsion for satellites and spacecraft: Established technologies and novel approaches," Plasma Sources Sci. Technol. **25**, 033002 (2016).
[2]D. M. Goebel and I. Katz, *Fundamentals of Electric Propulsion: Ion and Hall Thrusters*, JPL Space Science and Technology Series (Wiley, 2008) pp. 243–315.
[3]C. Drobny, F. Nurmberger, and M. Tajmar, in *Proceedings of the 5th Space Propulsion Conference*, SP paper 2016-3124751 (Rome, Italy, 2016).
[4]G. C. Potrivitu, R. Joussot, and S. Mazouffre, "Influence of anode position on discharge modes of a LaB_6 cathode in diode configuration," Vacuum **151**, 122–132 (2018).
[5]Y. Qin, K. Xie, and J. Ouyang, "Measurements and analysis of potential oscillations near the hollow cathode," Procedia Engineering **185**, 17–23 (2017).
[6]C. C. Farnell, J. D. Williams, and C. C. Farnell, "Comparison of hollow cathode discharge plasma configurations," Plasma Sources Sci. Technol. **20**, 025006 (2011).
[7]K. K. Jameson, D. M. Goebel, and R. M. Watkins, "Hollow cathode and thruster discharge chamber plasma measurements using high-speed scanning probes," in *Proceedings of the 29th International Electric Propulsion Conference*, IEPC paper 2005-269 (Princeton, NJ, 2005).
[8]H. R. Kaufman, *Technology of Electron-Bombardment Ion Thrusters*, Advances in Electronics and Electron Physics, Vol. 36 (Academic Press, New-York, 1974) pp. 265–373.
[9]M. J. Mandell and I. Katz, "Theory of hollow cathode operation in spot and plume modes," in *Proceedings of the 30th Joint Propulsion Conference*, AIAA paper 94-3134 (Indianapolis, In, 1994).
[10]S. D. Grishin and L. V. Leskov, *Electric Rocket Thrusters of Space Apparatus* (Mashinostroenie, Moscow (in Russian), 1989).
[11]R. Joussot, L. Grimaud, and S. Mazouffre, "Examination of a 5 A-class cathode with a LaB_6 flat disk emitter in the 2 A-20 A current range," Vacuum **146**, 52–62 (2017).
[12]Z. Ning, D. Yu, H. Li, and G. Yan, "Effect of the hollow cathode heat power on the performance of an Hall-effect thruster," Plasma Sci. Technol. **11**, 194–199 (2009).
[13]R. L. Washeleski and L. B. King, "Characterization of the plasma plume from a LaB_6 cathode: A comparison of probe techniques," in *Proceedings of the 45th Joint Propulsion Conference*, AIAA paper 2009-5199 (Denver, CO, 2009).
[14]L. Grimaud, A. Pétin, J. Vaudolon, and S. Mazouffre, "Perturbations induced by electrostatic probe in the discharge of Hall thrusters," Rev. Sci. Instrum. **87**, 043506 (2016).
[15]J. M. Lafferty, "Boride cathodes," J. Appl. Phys. **22**, 299–309 (1951).
[16]K. Kubota, Y. Oshio, H. Watanabe, S. Cho, Y. Ohkawa, and I. Funaki, "Numerical and experimental study on discharge characteristics of high-current hollow cathode," in *Proceedings of the*

52nd Joint Propulsion Conference, AIAA paper 2016-4628 (Salt Lake City, UT, 2016).
[17]D. Pedrini, R. Albertoni, F. Paganucci, and M. Andrenucci, "Experimental characterization of a lanthanum hexaboride hollow cathode for five-kilowatt-class Hall thrusters," J. Propul. Power **32**, 1557–1561 (2016).
[18]D. M. Goebel, K. K. Jameson, I. Katz, and I. G. Mikellides, "Potential fluctuations and energetic ion production in hollow cathode discharges," Phys. Plasmas **14**, 103508 (2007).
[19]R. B. Abernethy, R. P. Benedict, and R. B. Dowdell, "ASME measurement uncertainty," J. Fluids Eng. **107**, 161–164 (1985).
[20]S. J. Kline and F. A. McClintock, "Describing uncertainties in single sample experiments," Mech Eng **75**, 3–8 (1953).
[21]R. P. Benedict, *Fundamentals of temperature, pressure and flow measurements* (John Wiley & Sons, New York, 1984).
[22]M. Domonkos, A. Gallimore, G. Williams Jr, and M. Patterson, "Low-current hollow cathode evaluation," in *Proceedings of the 35th Joint Propulsion Conference*, AIAA paper 99-2575 (Los Angeles, CA, 1999).
[23]T. M. Jack, S. W. Patterson, and D. G. Fearn, "The effect of the keeper electrode on hollow cathode characteristics," in *Proceedings of the 36th Joint Propulsion Conference*, AIAA paper 2000-3533 (Huntsville, AL, 2000).
[24]R. Albertoni, M. Andrenucci, D. Pedrini, and F. Paganucci, "Preliminary characterization of a LaB_6 hollow cathode for low-power Hall effect thrusters," in *Proceedings of the 33rd International Electric Propulsion Conference*, IEPC paper 2013-137 (Washington D.C., 2013).
[25]S. Sakai, T. Katayama, J. Aoyagi, and H. Takegahara, "Discharge modes and characteristics of hollow cathode," in *Proceedings of the 30th International Electric Propulsion Conference*, IEPC paper 2007-215 (Florence, Italy, 2007).
[26]K. Nishiyama, Y. Shimizu, I. Funaki, H. Kuninaka, and K. Toki, "Ground chamber measurements of the electromagnetic emissions from the Hayabusa ion engine," J. Propul. Power **23**, 513–521 (2007).
[27]I. G. Mikellides, I. Katz, D. M. Goebel, and K. K. Jameson, "Evidence of nonclassical plasma transport in hollow cathodes for electric propulsion," J. Appl. Phys. **101**, 063301 (2007).
[28]B. A. Jorns, I. G. Mikellides, and D. M. Goebel, "Ion acoustic turbulence in a 100-A LaB_6 hollow cathode," Phys. Rev. E **90**, 063106 (2014).
[29]B. A. Jorns, C. Dodson, D. M. Goebel, and R. Wirz, "Propagation of ion acoustic wave energy in the plume of a high-current LaB_6 hollow cathode," Phys. Rev. E **96**, 023208 (2017).
[30]G. A. Csiky, "Measurements of some properties of a discharge from a hollow cathode," NASA Technical Note D-4966 (1969).
[31]R. Albertoni, P. Rosseti, F. Paganucci, and M. Andrenucci, "A reduced-order model for low-current orificed hollow cathodes," in *Proceedings of the 3rd Space Propulsion Conference*, paper SP-2012-2349890 (Bordeaux, France, 2012).
[32]J. Heberlein, J. Mentel, and E. Pfender, "The anode region of electric arcs: a survey," J. Phys. D: Appl. Phys. **43**, 023001 (2009).
[33]G. Sary, R. Joussot, L. Grimaud, L. Garrigues, S. Mazouffre, B. Laurent, C. Boniface, S. Oriol, and F. Masson, "Experimental and numerical investigations of a 5A-class cathode with a LaB_6 flat disk emitter in the 2 A–20 A current range," in *Proceedings of the 35th International Electric Propulsion Conference*, IEPC paper 2017-486 (Atlanta, GA, 2017).
[34]D. M. Goebel, K. K. Jameson, R. M. Watkins, I. Katz, and I. G. Mikellides, "Hollow cathode theory and experiment. I. plasma characterization using fast miniature scanning probes," J. Appl. Phys. **98**, 113302 (2005).
[35]V. Vekselman, Y. E. Krasik, S. Gleizer, V. T. Gurovich, A. Warshavsky, and L. Rabinovich, "Characterization of a heaterless hollow cathode," J. Propul. Power **29**, 475–486 (2013).
[36]S. Mazouffre, "Laser-induced fluorescence diagnostics of the cross-field discharge of hall thrusters," Plasma Sources Sci. Technol. **22**, 013001 (2013).
[37]S. Mazouffre, *Laser-induced fluorescence spectroscopy applied to electric thrusters*, edited by T. Magin, STO-AVT-VKI Lecture series, Vol. 263 (Von Karman Institute, Brussels, 2016) pp. 10–26.
[38]L. Grimaud and S. Mazouffre, "Ion behavior in low-power magnetically shielded and standard unshielded Hall thruster," Plasma Sources Sci. Technol. **26**, 055020 (2017).
[39]K. Dannenmayer, S. Mazouffre, P. Kudrna, and M. Tichý, "The time-varying electron energy distribution function in the plume of a Hall thruster," Plasma Sources Sci. Technol. **23**, 065001 (2014).
[40]G. Giono, J. T. Gudmundsson, N. Ivchenko, S. Mazouffre, K. Dannenmayer, D. Loubère, L. Popelier, M. Merino, and G. Olentsenko, "Non-Maxwellian electron energy probability functions in the plume of a SPT-100 Hall thruster," Plasma Sources Sci. Technol. **27**, 015006 (2018).
[41]J. G. J. Williams, T. B. Smith, M. T. Domonkos, A. D. Gallimore, and R. P. Drake, "Laser-induced fluorescence characterization of ions emitted from hollow cathodes," IEEE T. Plasma Sci. **28**, 1664–1675 (2000).
[42]C. Dodson, B. Jorns, and R. E. Wirz, "Ion acoustic wave propagation and heating in a high-current hollow cathode plume," in *Proceedings of the 35th International Electric Propulsion Conference*, IEPC paper 2017-398 (Atlanta, GA, 2017).
[43]V. J. Friedly and P. J. Wilburt, "High current hollow cathode phenomena," J. Propul. Power **24**, 635–643 (2008).
[44]I. G. Mikellides and I. Katz, "Wear mechanisms in electron sources for ion propulsion, 1: Neutralizer hollow cathode," J. Propul. Power **24**, 855–865 (2008).
[45]S. E. Cusson, B. A. Jorns, and A. Gallimore, "Ion acoustic turbulence in the hollow cathode plume of a Hall effect thruster," in *Proceedings of the 24th Joint Propulsion Conference*, AIAA paper 2018-4509 (Cincinnati, OH, 2018).
[46]J. R. Brophy and C. E. Garner, "Tests of high current hollow cathodes for ion engines," in *Proceedings of the 24th Joint Propulsion Conference*, AIAA paper 88-2913 (Boston, MA, 1988).
[47]M. J. Druyvesteyn, "Der Niedervoltbogen," Zeitschrift für Physik **64**, 781–798 (1930).
[48]V. A. Godyak, R. B. Piejak, and B. M. Alexandrovich, "Measurements of electron energy distribution in low-pressure RF discharges," Plasma Sources Sci. Technol. **1**, 36–58 (1992).
[49]V. A. Godyak and V. I. Demidov, "Probe measurements of electron-energy distributions in plasmas: what can we measure and how can we achieve reliable results?" J. Phys. D: Appl. Phys. **44**, 233001 (2011).
[50]V. I. Demidov, S. V. Ratynskaia, and K. Rypdal, "Electric probes for plasmas: The link between theory and instrument," Rev. Sci. Instrum. **73**, 3409–3439 (2002).
[51]D. A. Herman and A. D. Gallimore, "Discharge cathode electron energy distribution functions in a 40-cm next-type ion engine," in *Proceedings of the 41st Joint Propulsion Conference*, AIAA paper 2005-4252 (Tucson, AZ, 2005).
[52]T. K. Popov, M. Dimitrova, P. Ivanova, E. Hasan, J. Horáček, R. Dejarac, J. Stöckel, V. Weinzettl, and J. Kovačič, "Langmuir probe evaluation of the plasma potential in tokamak edge plasma for non-maxwellian EEDF," Contrib. Plasma Phys. **54**, 267–272 (2014).
[53]B. M. Reid and A. D. Gallimore, "Langmuir probe measurements in the discharge channel of a 6-kW Hall thruster," in *Proceedings of the 44th Joint Propulsion Conference*, AIAA paper 2008-4920 (Hartford, CT, 2008).
[54]M. C. M. V. de Sanden, J. M. de Regt, and D. C. Schram, "The behaviour of heavy particles in the expanding plasma jet in argon," Plasma Sources Sci. Technol. **3**, 501–510 (1994).
[55]L. Cassady and E. Choueiri, "Lithium-fed hollow cathode theory," in *Proceedings of the 40th Joint Propulsion Conference*, AIAA paper 2004-3431 (Fort Lauderdale, FL, 2004).